Experimental Characterization of Compression Failure Mechanism Initiation and Growth in Notched Carbon Fiber Reinforced Composite Specimens

Stephen Clay[1‡], Wesley Ault[2], Alex Faupel[3], Caglar Oskay[3], Philip Knoth[1], Noam N.Y. Shemesh[4], Rami Haj-Ali[5], Uri Breiman[5], Ido Meshi[5], Ofir Shor[6]

Abstract

This paper describes an experimental investigation to evaluate the compression failure mechanisms of kink banding, splitting, and delaminations under non-standard quasi-static loading of laminated carbon fiber reinforced composites. Tests were performed on double-edge notch compression (DENC) specimens to observe microscopic compressive damage initiation and progression. Acoustic emission results from specimens loaded to failure were used to define ranges of static stress associated with different forms of damage. Subsequent tests were interrupted at these stress intervals and results obtained from multiple inspection techniques provide quantified characterization of failure mechanism initiation and growth as a function of applied load level. Optical images of the exterior surfaces, micrographs of the laminate thickness generated via a grind/polish procedure, and postmortem X-ray computed tomographs provide detailed information on the 3D morphology and evolution of failure mechanisms in the laminate. Key failure characteristics include interior kink bands, surface ply splitting, and delaminations at two different types of interfaces. Kink bands are only present near ultimate failure while splitting and delamination initiate at approximately 50% lower stress levels. The experimental observations provide insight into the critical and subcritical nature of these failure mechanisms and their possible interactions in a multidirectional laminate under compression loading.

Keywords

Polymer-matrix composites (PMCs), mechanical properties (authors nominate “compression” as a keyword in place of “mechanical properties”), acoustic emission, CT analysis

[1‡] Corresponding: stephen.clay.2@us.af.mil, 2790 D St, Wright Patterson AFB, OH, 45433, USA
[2] Booz Allen Hamilton, Beavercreek, OH, USA
[3] Department of Civil Engineering, Vanderbilt University, Nashville, TN, USA
[4] Israel Air Force, Israel
[5] School of Mechanical Engineering, Tel Aviv University, Israel
[6] Rafael Advanced Defense Systems Ltd., Haifa, Israel

Introduction

The strength of aligned-fiber composites under compression has been measured to be up to 60% lower than its tensile strength [1,2]. The major difference in the failure mechanism between compression and tension, which also makes failure in compression that much harder to understand, is the formation of kink bands with aligned-fiber composites under compression. Detailed compression experiments of notched and unnotched carbon fiber reinforced polymer panels have been critical for a better understanding of the kink band formation process [1-5]. It has been established that this process initiates from a material imperfection, whether that be fiber misalignment [6-8], voids in resin pockets [9], or geometrical properties such as holes [3, 10-12], or notches [5, 13-15]. The localized compressive and axial-shear stresses reduce the lateral support which leads to instability that results in microbuckling of the fibers [16-17]. In multi-directional laminates, the kink band usually occurs in the plies parallel to the loading direction (i.e., in the zero-degree plies), and it is often accompanied by delamination of the adjacent plies and/or by intralaminar splitting [1, 9, 15]. In the case of notched or open-hole laminated composites, splitting in the zero-degree and forty-five-degree plies is also observed [18-20].

Although these works provided valuable insights into the compressive strength of the composite, it is challenging to obtain the in-situ failure at the appearance of kink bands due to the unstable crack propagation which results in catastrophic failure. A more recent specimen design, which allows gradual crack failure to propagate, the double-edge-notch-compression (DENC) specimen was investigated by Catalanotti et al. [13] and refined by Bergan et al. [15]. Similar to Lee and Soutis [18] and Bishara and Vogler [20], both works which experimented on cross-ply laminated DENC specimens argued that splitting occurs prior to the kink band formation, followed by delamination, leading to macro-buckling and specimen collapse. However, their conclusions were partially based on numerical analysis, and the failure sequence was not observed directly.

The research described in this paper considers a modified DENC specimen layup design and testing configuration to help better characterize the formation of kink bands prior to catastrophic failure. The ultimate purpose of this paper is to describe the details of the interrupted DENC specimen test campaign and to provide unique observation of the formation of ply splitting, delamination, and kink band formation to help better understand the dynamic mechanisms of compression failure evolution. The novel contribution of this manuscript is the experimental observation of time/load-dependent evolution of failure mechanisms (kink bands, splits, delaminations) under compression loading and assessment of failure mechanism interactions throughout the loading process. The composite layup, specimen geometry, test procedure, test results, and inspection methods are described in detail in subsequent sections of this paper, along with a conclusion with suggestions on how to develop these findings further.

Test Specimen Design and Fabrication

Experiments were conducted on non-traditional DENC specimens using a Combined Loading Compression (CLC) test fixture. The laminate was hand-laid and autoclave cured from IM7/977-3 carbon/epoxy unidirectional pre-impregnated tape with a stacking sequence of $[0_3/+45/-45/90/0]_s$, as shown in the cross-section presented in Figure 1. The proposed specimen thickness follows the recommendations set by [19] to avoid Euler buckling. The overall dimensions were inspired by [13, 15] who examined the effect of the specimen size on the strength. The layup was specifically selected from a screening trial in which the following three layups were tested: $[0_4/+45/-45/90]_s$, $[0_3/+45/-45/90/0]_s$, and $[0_2/+45/-45/90/0_2]_s$. In the trial, the surface plies were aligned in the loading direction with the expectation of directly observing kink band formation and propagation. It was found that all of the layups developed kink bands, but the selected stacking sequence was the only one that produced a stable crack-like damage progression so that the test could be stopped and the sub-critical damage examined, as can be seen in Figure 2. Based on the optical images, it appears that this surface damage was more severe and consisted of more extensive fiber damage compared to the kink bands observed on the internal plies during subsequent testing. This extensive amount of visual surface damage was only observed on a total of five test specimens during this study.

The same material and fabrication process were used to make all DENC test coupons. Figure 3 shows a schematic of the test specimen showing the geometry and dimensions. Each specimen had a nominal thickness of approximately 2.0 mm in the gage section. Special care was taken to ensure the two notches were machined without introducing damage locally in the gage section of the specimen. A machining study was performed by machining notches with different milling parameters. These notches were then examined under a microscope, and the following parameters gave the best notch quality without inducing any damage into the composite. The end mill selected had two flutes, a diameter of 0.508 mm, and a reach of 2.54 mm. The spindle speed was approximately 12,000 RPM with a feed rate of 50.8 mm/min. The depth of cut was 0.0508 mm per pass, and the composite sample was backed with a G10 epoxy board. This machining process resulted in a notch tip of 0.508 mm. Following machining of the notched specimens, tabs were bonded to both ends of the specimens using Hysol EA9394, a two-part structural paste adhesive.

Test Apparatus

The specimens were tested under room temperature ambient conditions using a 90 kN MTS Instru-Met Corporation electromechanical testing machine. Each specimen was tested using the ASTM D6641 [21] combined loading compression test fixture which can be seen in Figure 4a. As specified in the standard, a constant displacement rate of 1.3 mm/min was applied to the specimens for all tests while recording force and crosshead displacement at 10 Hz from the test machine.

Besides the test machine data acquisition, a virtual extensometer and Acoustic Emission (AE) system were also used during each test. Local strains and displacements across the gage section between the notches were measured using an MTS virtual extensometer (VE) system. Acoustic events were measured using a Mistras AE system and four AE sensors which were placed in the gage section of each specimen above and below each of the notches near the radius end.

Virtual Extensometer (VE)

The VE system used a two-dimensional Allied Vision Manta digital camera to accurately track the relative displacement between two black dots that were placed on the specimen, as shown in Figure 4b. Images were captured at 10 Hz and processed using a live MTS Auxiliary System Controller. Local strains and displacements that are displayed in the stress-strain plots in this manuscript were calculated with advanced Video Gauge software.

Acoustic Emission (AE)

A Micro-II digital acoustic emission system produced by Physical Acoustics Corporation was used to detect and record the acoustic energy emitted by the composite material during matrix cracking, delamination, fiber fracture, and kink band formation. Four acoustic sensors were bonded to the specimen surface above and below the notch tips as shown in Figure 4c. An acoustic signal amplitude threshold of 40 dB with a 6 dB band permitted the detection of valid material failures while filtering out ambient laboratory noise. The timing parameters used during this exercise were a peak definition time of 30 μs, a hit definition time of 150 μs, a hit lockout time of 300 μs, and a maximum duration of 100 ms. The acoustic wave velocity for this specific composite makeup was calculated to be roughly 7,366 m/sec. The AE sensors themselves were located approximately 3.175 mm from the edge of each specimen and approximately 1.27 mm above and below each notch.

Optical Imaging Camera

Optical images of the DENC specimen face between the two notches were captured throughout the test at 100 Hz using a single Unibrain monochrome 5 MP industrial digital camera with a c-mounted Infinity video microscope lens. This arrangement provided a 50 mm working distance and a 3 mm field of view (FOV). Fiber-optic lighting was used to illuminate the specimen surface during these inspections. Image acquisition was accomplished with software provided with the Unibrain camera and time synced with the DIC and test frame systems. The imaging system saved timestamped images which provided a history of the experiment.

These images were monitored in real-time to visually track surface damage like splitting and cracking. In a few cases, the experimental team was able to track a crack growing from one notch to the other and stop the test to prevent catastrophic compression failure. During the early characterization phase, the test was also stopped when surface splitting was optically observed with digital imaging in order to characterize damage initiation sequences.

X-ray Microcomputed Tomography

Microcomputed Tomography (μCT) scans were performed on the damaged composite specimens using a Zeiss Xradia Versa 620 X-ray Microscope (XRM) system. The system was equipped with a 160 kV transmission target X-ray source, a flat-panel detector, and a series of optical objectives which allowed obtaining a wide range of magnifications. Scanning times ranged from 3 to 14 hours, depending on magnification and the regions scanned. Specimens were scanned with and without dye penetrant.

Grind/Polish Micrograph Process

A grind/polish micrograph process was conducted on a select number of tested specimens to quantitatively characterize kink band initiation and growth. These results, coupled with X-ray CT, helped confirm damage formation within the tested specimens at intermediate loads prior to failure. A Measuring Microscope MM-60 table-top microscope produced by Nikon, along with Nikon NIS-Elements D software and a Nikon DS-Fi2 camera were used to examine and capture cross-sectional images of the specimens. An Automet 2 Power Head with an Ecomet 3 Grinder/Polisher produced by Buehler was used to grind and polish specimens, as shown in Figure 5, at approximately 1.27 mm increments up to the notch tip and at finer increments when in the damaged region. The micrographs and X-ray CT radiographs show cross-sections of the specimen within the gage section between the two notches that propagate from one notch to the other. This data allows observation of surface ply splits, delaminations, and kink band initiation and growth.

Experimental results and discussion

Double-Edge Notch Compression Testing Methodology

A total of 44 compression tests were performed on the $[0_3/+45/-45/90/0]_s$ DENC specimens. These tests were conducted on all specimens using the standards established in ASTM D6641 [21] and monitored using a virtual extensometer and an acoustic emission system. For a select number of specimens, both X-ray CT radiographs and micrographs were taken in the gage section between the two notches in order to characterize the internal damage and formation of kink bands during compression. In Clay et al. [22], the unidirectional ply-level properties of this same IM7/977-3 material system were obtained using the ASTM standards listed in Table 1. These properties helped determine the test parameters.

The compression tests were divided into a baseline phase and a damage characterization phase. During the baseline phase, three specimens were loaded to complete failure without interruption in order to determine the ultimate stress and the stress at which damage initiated and propagated. Based on the baseline results, the stress intervals at which the characterization tests were interrupted were determined. Stress is calculated by dividing the measured load from the test machine by the total cross-sectional area (as opposed to the net cross-sectional area between the notches). This metric was selected in order to provide a consistent relative comparison of damage for different load levels in a region of highly non-uniform stress across the gage section and to be consistent with published literature [Ref 15 - Fig 9].

Baseline tests

Acoustic emission testing was performed on three baseline DENC specimens to help define ranges of static stress at which different forms of damage was occurring. The nominal compressive stress and cumulative absolute energy versus strain for these tests are shown in Figure 6. The cumulative absolute energy is the integration of the absolute energy with respect to acoustic events, while the absolute energy is a true measure of energy for each acoustic waveform recorded. The strain used was the localized measurement from the virtual extensometer. Based on these results, two regions were defined for high fidelity damage

characterization. The first level, from 175 to 210 MPa, was selected in order to characterize the damage that triggered the lower energy AE events, while the second level, from 210 MPa and above, was selected based on the higher energy AE events.

Characterization tests: Level 1

Based on the AE results from the baseline tests, the first level of characterization testing was conducted within the nominal stress range of 175 and 210 MPa. After passing 175 MPa, a test was stopped for detailed inspection if there was visual observation of ply splitting on the surface of the specimen or if an individual acoustic emission event occurred with an energy on the order of 10^{-14} J or higher. The nominal compression stress and AE responses for the seven Level 1 characterization tests are shown in Figure 7.

During testing, digital cameras were used to observe the specimen surfaces as previously described. Figure 8 displays representative optical images of surface ply splitting commonly seen on Level 1 test specimens. Although surface ply splitting is challenging to capture real-time, it was observed on approximately 75% of the Level 1 specimens prior to stopping the tests for more detailed inspections. Splitting was initially observed in the nominal stress range of 150 to 175 MPa with an average length among 6 specimens of 1.66 mm (Coefficient of Variation, CV 35.5%). It can be seen that the split emanated from near the notch tip and extended toward the upper or lower edge of the test specimen. The images obtained for the Level 1 specimens do not clearly show whether or not the split extended through the thickness of the zero-degree plies.

In order to further characterize the internal damage at these low stress levels, some of the test specimens were ground, polished, and micrographed according to the procedure described above. Figure 9 shows representative micrographs near the notch tips of two Level 1 test specimens. There was no indication of kink band formation or other type of damage up to stress levels of 210 MPa. Based on the combination of the surface images and the internal micrographs, it is concluded that the Level 1 acoustic events were not the result of kink band formation but were caused solely by surface ply splitting.

Characterization Tests: Level 2

Based on the baseline AE results, the second level of characterization testing was conducted in the nominal stress range of 210 MPa and above. Fifteen tests were conducted in order to characterize kink band formation and growth as a function of applied compression stress. After the test specimens exceeded a stress level of 210 MPa, the tests were stopped for detailed inspection at the occurrence of an individual acoustic emission event with an energy on the order of 10^{-13} J or higher or if a visually observable apparent crack appeared on the specimen surface. The acoustic level of 10^{-13} J was selected as the threshold based on past experience where lower energy events did not result in detectable damage within the composite. The nominal compression stress and AE responses for the Level 2 characterization tests are shown in Figure 10.

Similar to the specimens from the Level 1 characterization tests, the majority of the Level 2 specimens experienced visually detectable surface ply splitting prior to stopping the tests for detailed inspections as shown in Table 2. The difference is that once the splitting was observed, the tests continued until a significant AE event or horizontal surface crack appeared. Four of the fifteen Level 2 specimens had horizontal surface cracks emanating from one of the notch tips starting at a stress level of 234 MPa.

Figure 11 shows a schematic of the test specimen coordinate axes and four images of a Level 2 characterization specimen that was incrementally ground, polished, and micrographed after it was loaded to a nominal stress of 294 MPa. This same process was repeated on several other specimens at different stress levels in order to thoroughly characterize kink band growth as a function of compression stress. Figure 11(b-e) depict a cross-sectional view through the thickness of the specimen at increasing distances from one of the notch tips. Noticeable damage in the center zero-degree plies and adjacent forty-five degree plies can be seen in Figure 11b at a close distance of 0.15 mm from the notch tip. In this specimen, the outer zero-degree plies do not exhibit any damage. The remaining images focus on the region between 2 and 3 mm from the notch. At 2.2 mm (Figure 11c), a well-established kink band can be seen in the center zero-degree plies, but no other damage is evident. The center kink band is barely visible at a depth of 2.6 mm (Figure 11d) while no

damage is seen at a depth of 3.0 mm (Figure 11e). These results indicate that the length of the kink band is between 2.6 and 3.0 mm.

Thorough investigation of kink band formation and growth using this grind/polish/micrograph approach was conducted on six of the fifteen Level 2 characterization specimens. Figure 12 shows a sample image of a kink band in the center zero-degree plies of one of the Level 2 specimens with the angle (α) and width (w) annotated. Table 3 shows the results of the microscopic kink band characterization. Five of the six specimens were tested to at least 90% of the average ultimate stress (318 MPa) found during baseline testing. Similar to what was extracted from the images in Figure 11, the kink band length from the notch tip is given as a range rather than a single value since it was determined from a series of micrographs at discrete distances. The maximum possible kink band lengths were found to be in the range of 1.5 to 3 mm, which is approximately 10 to 25% of the distance between the two notches. Similar kink bands may have formed from the opposite notch, which would indicate that the progression across the width of the specimen could be as high as 50% of the gage section but is likely significantly less. The measured values of both the width and angle of the kink bands were found to be very consistent. The average width was measured to be 0.025 mm (CV 14.7%) while the average angle was found to be 23.2 degrees (CV 9.1%). In the previously published literature, kink band morphology has been measured in other notched carbon-fiber/epoxy laminates containing nonzero-degree plies. These examples include 17 μm/s compression loading of multidirectional (various layups consisting of forty-five, zero, and ninety-degree plies) open hole T800/924C specimens additionally supported with an anti-buckling device [2], and 1 μm/s compression loading of cross-ply single-edge notched IM7/8552 specimens [23]. The kink band length is observed at 20-30% of the unnotched width immediately prior to failure. Kink band widths and angles were observed in the ranges of 20-35 μm and 5-30 degrees, respectively.

Microcomputed tomography was used to inspect a damaged DENC specimen in order to better understand kink band interactions with other damage mechanisms such as splitting and delaminations. The specimen was previously loaded to a nominal compression stress of 292 MPa which is 92% of the average failure stress

of the baseline specimens. Internal damage is shown in the low magnification (0.395 μm to 7.55 μm voxel size) tomographs of Figure 13. It can be seen in Figure 13a that the outer zero-degree plies experienced ply splitting from both notch tips, which agrees with previous observations from optical imaging. No kink banding was evident on the outer plies and no splitting was observed at the notch in the inner zero-degree plies. Figure 13b shows that the forty-five degree plies were affected by the surface ply splits and experienced jagged and angled splitting/cracking at the notch tips. In the high magnification tomograph shown in Figure 14, it can be seen that kink bands formed within the jagged damage pattern in the forty-five-degree plies. Other experimental results using optical microscopy have shown kink bands propagating in exterior non-zero-degree plies in notched carbon-epoxy multidirectional laminates under compressive loading. In Sivashanker, 2001, [24] kink bands are visible in forty-five-degree plies in segments orthogonal to the fiber direction and are connected by much longer matrix cracks than visible in Figure 14. The result is what appears to be a jagged fracture path propagating transverse to the loading direction. No information is provided on splitting of the interior zero-degree plies. While a clear matrix crack is present close to the notch height in Figure 14, the damage does not propagate in the transverse direction from the end of that matrix crack. To our knowledge the jagged damage pattern observed in Figure 14 which aligns primarily with the splitting in the zero-degree plies has not been reported before and points to the effects of exterior zero-degree ply splitting on the DENC failure process. The split at the left notch in Figure 13a is longer than the jagged kink band damage in Figure 13b, which could indicate that the exterior ply splits caused stress redistribution and consequently this damage pattern in the forty-five-degree plies. No internal damage was detected in the ninety-degree ply shown in Figure 13c. Figure 13d shows a kink band protruding from the right notch tip. A more detailed description of the kink bands is given in Figures 15-16.

High magnification tomographs were obtained in the region of the kink band in the center zero-degree plies near the right notch tip as shown in Figure 15. In the specimen face-view tomograph of the center zero-degree plies shown in Figure 15a, it can be seen that the kink band initiated near the notch tip and grew toward the center of the test specimen. Very similar to the observations of notched cross-ply laminates in

Gutkin et al, 2010 [Section 4.1] [25], the kink band as shown in Figure 15a consists of multiple regions with varying angle and width. The root of the kink band is located off of the notch tip due to the shear concentration and subsequent splitting. From the root, a shear-driven fiber-compressive failure path forms at a nearly forty-five degree angle away from the notch and toward the center of the specimen. The kink band angle is shallower in the region where multiple fibers are rotated together. An intermediate kink band angle is due to fibers breaking in tension only on top of the rotated segments and an even more shallow angle exists further away from the notch where fibers break on two planes forming a kink band width of many fiber diameters. The location and direction of Figure 15 (b)-(g) is shown, with (b) being the farthest from the notch tip and (g) being the closest to the notch tip. It can be seen that location (b) is far enough from the notch tip that no damage is evident either in the form of a delamination or a kink band. Location (c) shows the first sign of a delamination that has formed between the center zero-degree and the ninety-degree ply. Figure (d) indicates that the delamination had grown and was fully established ahead of the kink band tip in Figure (e). At locations (f) and (g), which are closer to the notch tip, both the kink band and delamination were fully established.

To better visualize the cracks and internal damage, an additional tomography scan was performed using a zinc iodide dye-penetrant solution containing ZnI2 powder, water, isopropyl alcohol, and a wetting agent. Results from this scan are shown in Figure 16. Multiple forms of damage are present. First, a kink band is exhibited by a solid, opaque, crack-like feature that initiated at the notch in the central zero-degree plies and extended toward the center of the specimen. Multiple delaminations are shown as vertical fan-shaped features. These delaminations occurred on the +/- forty-five degree and zero/ninety-degree interfaces. The kink band is bound by delaminations at the interfaces between the zero-degree and ninety-degree plies.

Conclusions

The main objective of this study was to evaluate composite compression failure mechanisms under non-standard quasi-static loading, and in particular, identify compressive damage initiation and interlaminar damage progression in the characterization of kink band formation. For this reason, a novel experimental

method was developed which incorporated a unique test specimen design that enabled damage progression to be observed and kink band formation rate to be controlled for characterization at different intermediate load levels to catastrophic failure. In addition, an advanced test procedure that combined in-situ and post-test measurements provided insight into damage extent as a function of compression load.

Damage mechanisms that were recognized during the investigation include surface splitting, intralaminar cracking, delamination, fiber fracture, and kink bands. The kink bands were primarily observed in the central zero-degree plies, but they were also seen in the forty-five-degree plies. It is reasonable to assume that the former is the primary contributor to the strength loss, while the latter has a secondary effect. The observation that no other damage besides surface splitting was seen on the Level 1 specimens indicates that surface splitting occurred first. It should be noted that this conclusion is solely based on the stress states applicable to this DENC specimen configuration. At higher stress levels, kink bands within the forty-five degree plies and central zero-degree plies initiated and grew in the range of 75% to 100% of the ultimate stress. In this higher range, delamination and matrix cracking were also present. Damage initiated and fibers fractured to form kink bands but did not noticeably change the global mechanical response (i.e., the slope of the stress-strain curve) up to final failure. Ultimate failure was observed when the kink bands had propagated 1.5 - 3.0 mm from a notch tip.

Based on the experimental observations, it is challenging to determine the effects of underlying defects in the microstructure (e.g., fiber misalignment and inelastic matrix deformation) on kink band formation. However, it seems that transverse and longitudinal intra-ply matrix cracking, as well as delamination, contributed to a local loss of fiber support that may have stimulated a micro-buckling process that ended up with fiber fracture, forming the observed kink bands. However, CT scans and micrograph images in multiple sections of the examined specimens, as well as three dimensional micro-CT images, may provide information on the damage formation steps from initiation to final failure. In the specimens that were investigated, it is clearly evident that the initial failure mechanism is surface splitting emanating from the notch tip due to high stress concentration. The surface splitting, which is essentially transverse matrix cracking, caused a

redistribution of stresses within the specimen resulting in stress concentration relief in the volume surrounding the notch. As a result of matrix cracking (dominantly at the zero-degree plies), sub-critical kink bands formed in adjacent plies (dominantly forty-five degree plies) as well as delamination formation from the edges of the matrix cracks. It is reasonable to assume that as a result of local loss in fiber support induced by delamination, local micro-buckling of the fibers started to develop within the central zero-degree plies and resulted in the formation of kink bands after fiber fracture. The observations along different sections from the notch show that delaminations progressed deeper into the specimen than kink bands. This may provide implications of the damage propagation process in real-time. After the notch delamination and the middle kink band had formed, delamination continued to propagate toward the centerline of the specimen resulting in a continuous loss-of-support path for the kink band to follow while the load increased. Subcritical as well as critical damage mechanisms continued to grow until the remaining intact structure lost its load carrying capability.

In summary, this effort generated experimental data to provide unique evidence of the initiation and interaction of ply splitting, delamination, and kink bands as a function of the loading path up to complete failure. The results of this work may further contribute to the development of damage laws for these failure mechanisms, as well as computational methods and strategies for simulation of multidirectional laminates with notches. All results displayed are believed to accurately capture this unique formation of damage characteristics within a double-edge notched compression test and are suitable for future assessments.

Acknowledgements

The authors gratefully acknowledge the technical support provided by Messrs. Richard Polson and Scott Tursic in grinding, polishing, and micrograph generation for detailed microscale inspections. Gratitude is also extended to Mr. Jason Miller for creating high-quality notches in the test specimens. Finally, authors Caglar Oskay and Alex Faupel gratefully acknowledge the financial support of the Air Force Research Laboratory (AFRL SIRCA Award No: FA8650-640 19-2-2214).

References

1. Soutis C, Curtis PT, Fleck, NA. Compressive failure of notched carbon fibre composites. Proceedings of the Royal Society of London. Series A: Mathematical and Physical Sciences 1993; 440.1909: 241-256. http://doi.org/10.1098/rspa.1993.0014.

2. Vogler TJ, Kyriakides S. On the initiation and growth of kink bands in fiber composites: Part I. experiments. International Journal of Solids and Structures 2001; 38(15): 2639-2651. https://doi.org/10.1016/S0020-7683(00)00174-8.

3. Moran PM, Liu XH, Shih CF. Kink band formation and band broadening in fiber composites under compressive loading. Acta Metallurgica et Materialia 1995; 43(8): 2943-2958. https://doi.org/10.1016/0956-7151(95)00001-C.

4. Schultheisz CR, Waas AM. Compressive failure of composites, Part I: Testing and micromechanical theories. Progress in Aerospace Sciences 1996; 32(1): 1-42. https://doi.org/10.1016/0376-0421(94)00002-3.

5. BAZANT ZP, KIM JJH, DANIEL IM, BECQ-GIRAUDON E, ZI G. Size effect on compression strength of fiber composites failing by kink band propagation. International journal of fracture. 1999;95(1-4):103-141. doi:10.1023/A:1018640015465

6. Kyriakides S, Arseculeratne R, Perry EJ, Liechti K. On the compressive failure of fiber reinforced composites. International Journal of Solids and Structures 1995; 32(6-7): 689-738. https://doi.org/10.1016/0020-7683(94)00157-R.

7. Kyriakides S, Ruff AE. Aspects of the failure and postfailure of fiber composites in compression. Journal of Composite Materials 1997; 31(16): 1633-1670. https://doi.org/10.1177%2F002199839703101604.

8. Zhou HW, Yi HY, Gui LL, Dai GM, Peng RD, Wang HW, Mishnaevsky Jr L. Compressive damage mechanism of GFRP composites under off-axis loading: Experimental and numerical investigations. Composites Part B: Engineering 2013; 55: 119-127. https://doi.org/10.1016/j.compositesb.2013.06.007.

9. Sun Q, Zhou G, Guo H, Meng Z, Chen Z, Liu H, et al. Failure mechanisms of cross-ply carbon fiber reinforced polymer laminates under longitudinal compression with experimental and computational analyses. Composites Part B: Engineering 2019; 167: 147-160. https://doi.org/10.1016/j.compositesb.2018.12.041.

10. Suemasu H, Naito Y, Gozu K, Aoki Y. (2012). Damage initiation and growth in composite laminates during open hole compression tests. Advanced Composite Materials 2012; 21(3): 209-220. https://doi.org/10.1080/09243046.2012.723330.

11. Zhang D, Zheng X, Wu T. Damage characteristics of open-hole laminated composites subjected to longitudinal loads. Composite Structures 2019; 230: 111474. https://doi.org/10.1016/j.compstruct.2019.111474.

12. Takamoto K, Ogasawara T, Kodama H, Mikami T, Oshima S, Aoki K, et al. Experimental and numerical studies of the open-hole compressive strength of thin-ply CFRP laminates. Composites Part A: Applied Science and Manufacturing 2021; 145: 106365. https://doi.org/10.1016/j.compositesa.2021.106365.

13. Catalanotti G, Xavier J, Camanho PP. Measurement of the compressive crack resistance curve of composites using the size effect law. Composites Part A: Applied Science and Manufacturing 2014; 56: 300-307. https://doi.org/10.1016/j.compositesa.2013.10.017.

14. Allix O, Feld N, Baranger E, Guimard JM, Ha-Minh C. The compressive behaviour of composites including fiber kinking: Modelling across the scales. Meccanica 2014; 49(11): 2571-2586. https://doi.org/10.1007/s11012-013-9872-y.

15. Bergan AC, Jackson WC. Validation of a mesoscale fiber kinking model through test and analysis of double edge notch compression specimens. In: Proceedings of the American Society for Composites Conference, Seattle, Sep, 2018. NF1676L-29494.

16. Argon AS. Fracture of composites. Treatise of Materials Science and Technology 1972; v1: 79-114. Academic Press, New York. https://doi.org/10.1016/B978-0-12-341801-2.50007-2.

17. Budiansky B, Fleck NA. Compressive kinking of fiber composites: A topical review. Applied Mechanics Review 1994; 47(6S): S246-S250. https://doi.org/10.1115/1.3124417.

18. Lee J, Soutis C. Thickness effect on the compressive strength of T800/924C carbon fibre–epoxy laminates. Composites Part A: Applied Science and Manufacturing 2005; 36(2): 213-227. https://doi.org/10.1016/j.compositesa.2004.06.010.

19. Lee J, Soutis C. A study on the compressive strength of thick carbon fibre–epoxy laminates. Composites Science and Technology 2007; 67(10): 2015-2026. https://doi.org/10.1016/j.compscitech.2006.12.001.

20. Bishara M, Vogler M, Rolfes R. Revealing complex aspects of compressive failure of polymer composites–Part II: Failure interactions in multidirectional laminates and validation. Composite Structures 2017; 169: 116-128. https://doi.org/10.1016/j.compstruct.2016.10.091.

21. ASTM Standard D6641/D6641M (2016). Compressive Properties of Polymer Matrix Composite Materials Using a Combined Loading Compression (CLC) Test Fixture. ASTM International, West Conshohocken, PA, DOI: 10.1520/D6641_D6641M-16E02

22. Clay SB, Knoth PM. Experimental results of quasi-static testing for calibration and validation of composite progressive damage analysis methods. Journal of Composite Materials 2017; 51(10): 1333-1354.

23. Bergan AC, Garcea SC. In-situ observations of longitudinal compression damage in carbon-epoxy cross ply laminates using fast synchrotron radiation computed tomography. In: Proceedings of the American Society for Testing and Materials (ASTM) D30 Meeting, 2017. https://ntrs.nasa.gov/citations/20170010325

24. Sivashanker S. Damage propagation in multidirectional composites subjected to compressive loading. Metallurgical and materials transactions A, Physical metallurgy and materials science. 2001;32(1):171-182. doi:10.1007/s11661-001-0113-y

25. R. Gutkin, S.T. Pinho, P. Robinson, P.T. Curtis. On the transition from shear-driven fibre compressive failure to fibre kinking in notched CFRP laminates under longitudinal compression. Composites Science and Technology 2010, 70(8), 1223-1231, ISSN 0266-3538, https://doi.org/10.1016/j.compscitech.2010.03.010.

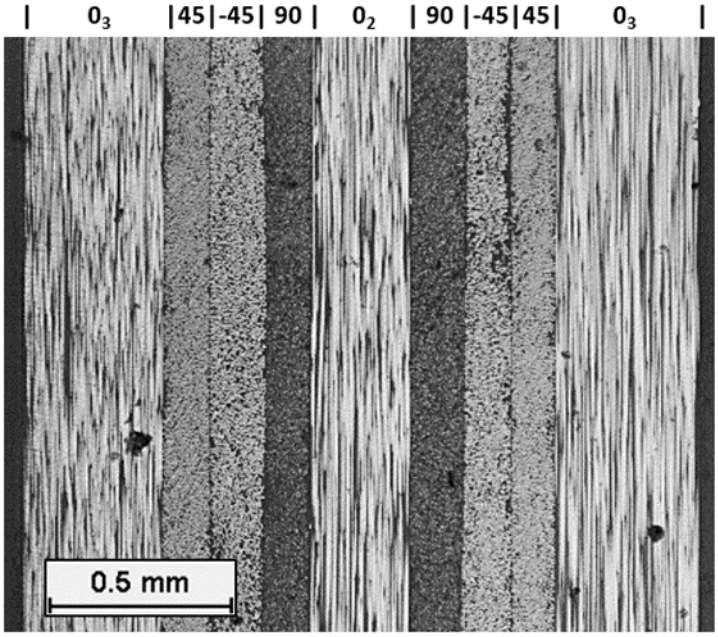

Figure 1. Micrograph showing fiber morphology of DENC specimen.

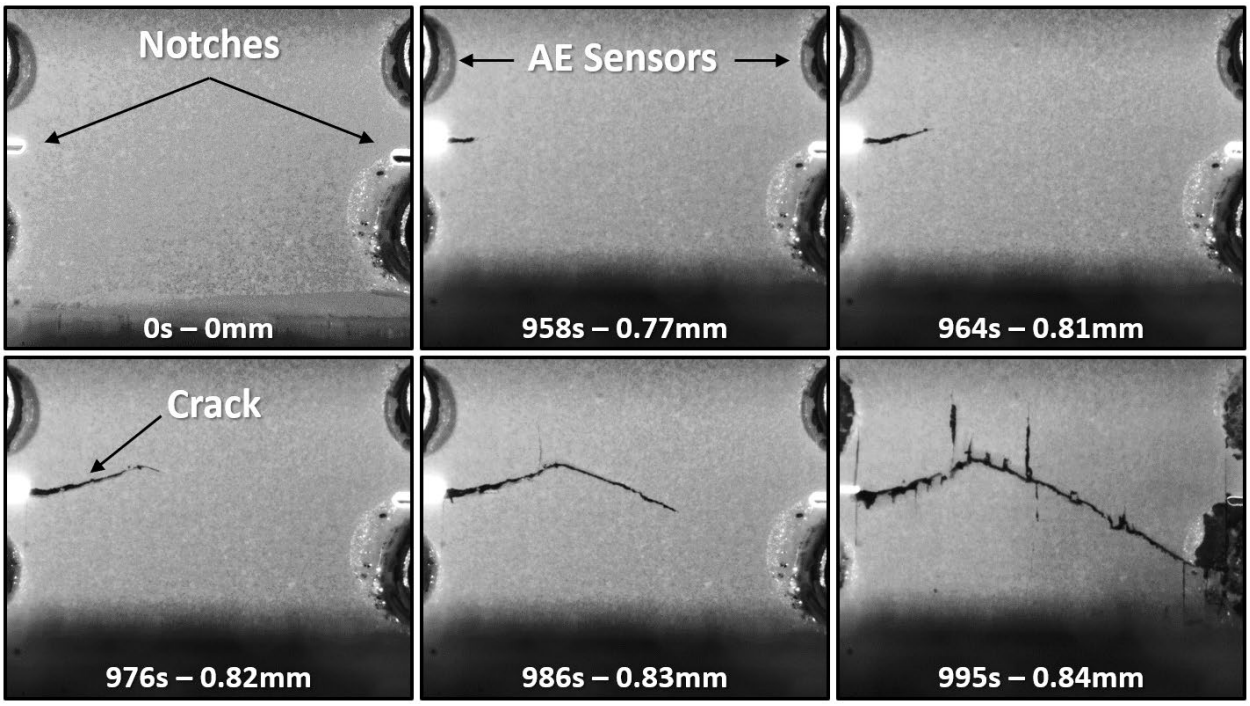

Figure 2. Optical images from the DENC screening test of progressive damage showing test time and crosshead displacement.

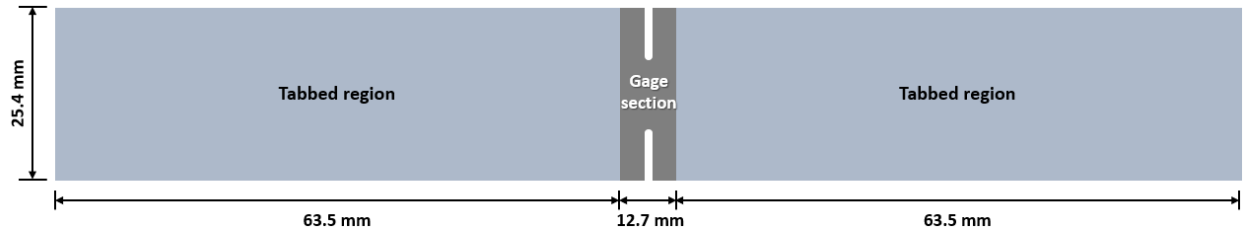

Figure 3. Geometry of the DENC Test Specimen. (Color on web only)

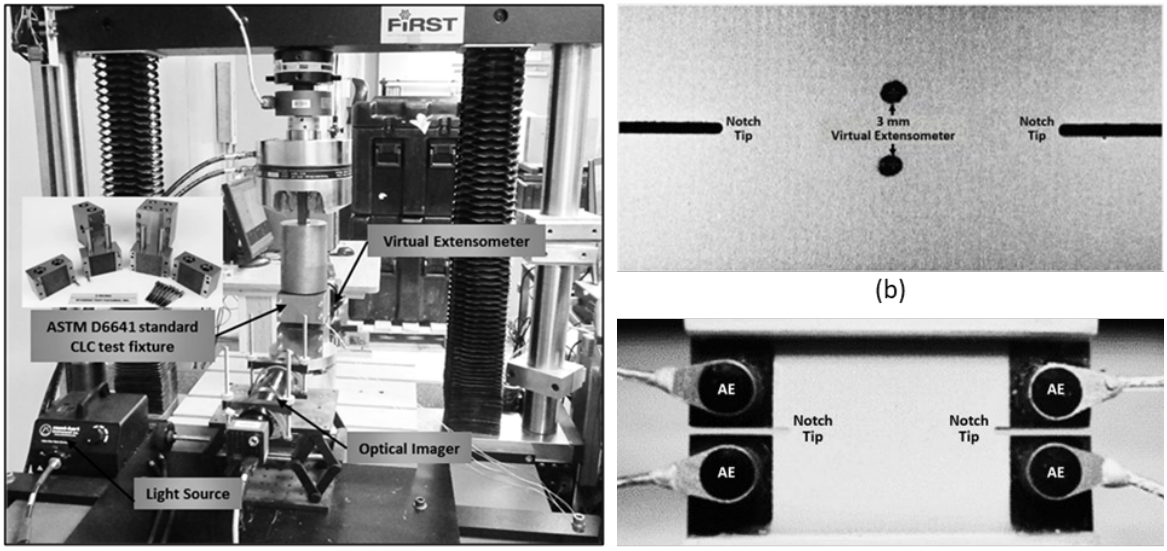

(a) (b) (c)

Figure 4. (a) DENC experimental test setup with the Four-Alignment Rod CLC fixture shown as a subset, (b) DENC specimen marked for VE data acquisition, and (c) Double-edge notch compression specimen with four acoustic emission sensors attached above and below each notch.

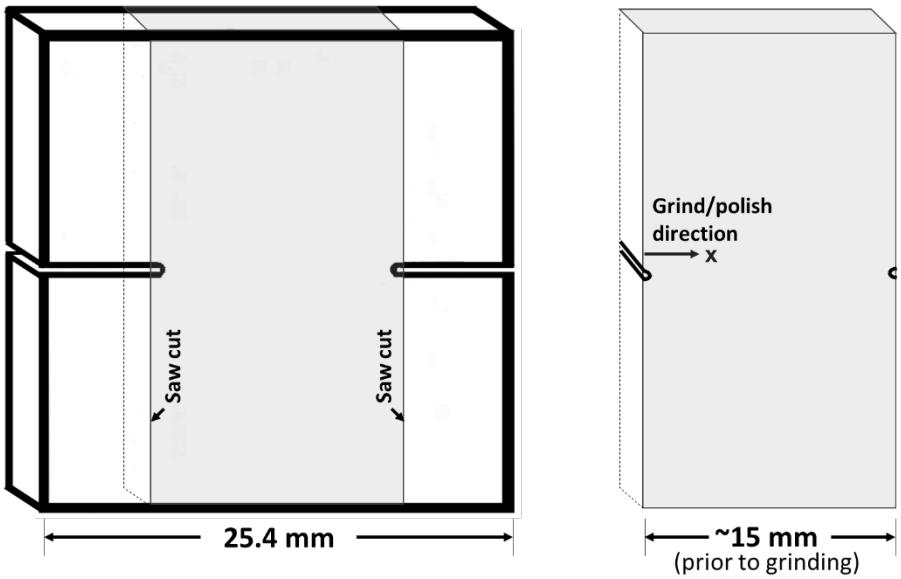

Figure 5. Incremental grinding/micrographing process.

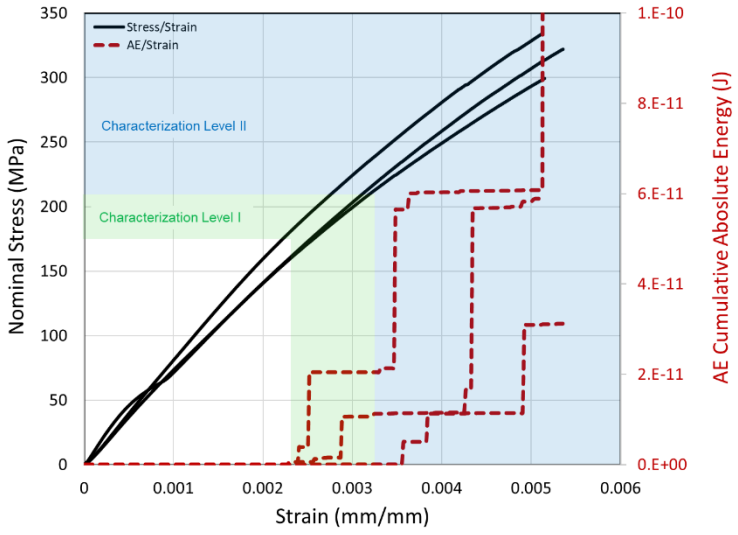

Figure 6. Nominal compression stress and AE responses of baseline DENC specimens. (Color on web only)

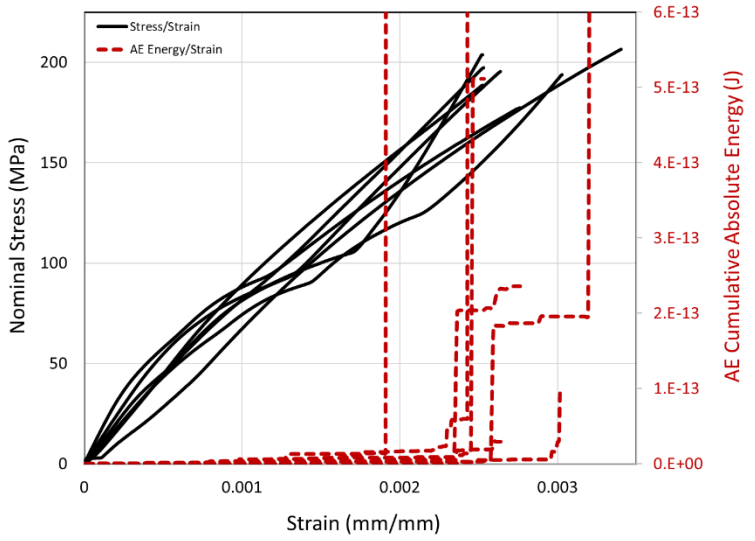

Figure 7. Nominal compression stress and AE responses for Level 1 characterization tests (color on web only)

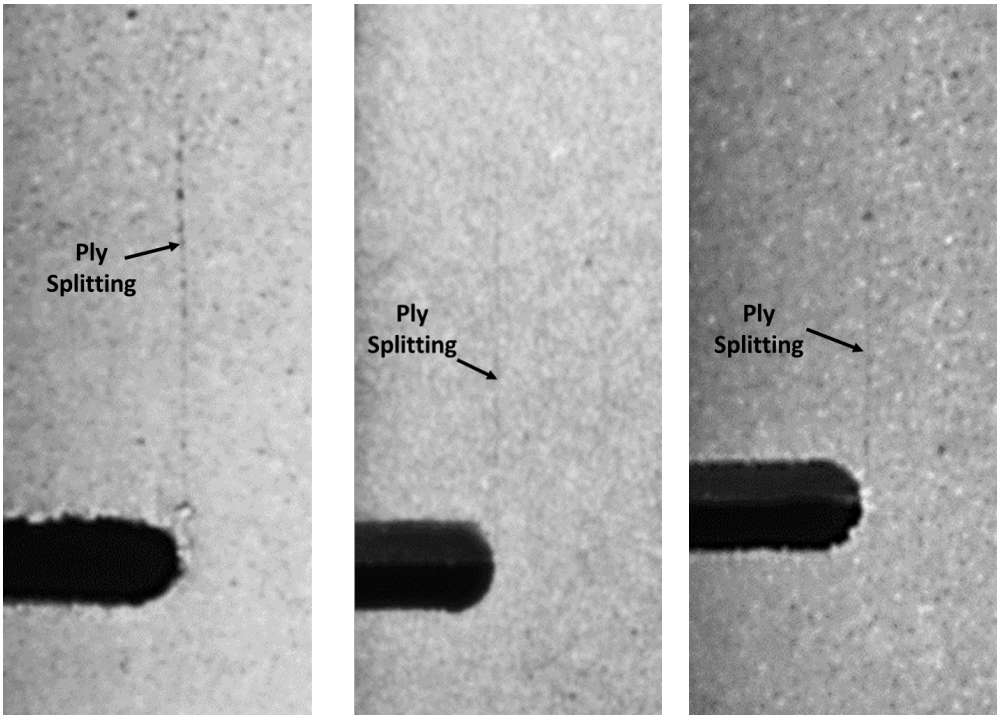

Figure 8. Digital images of surface ply splitting initiating from the notch tip in Level 1 test specimens

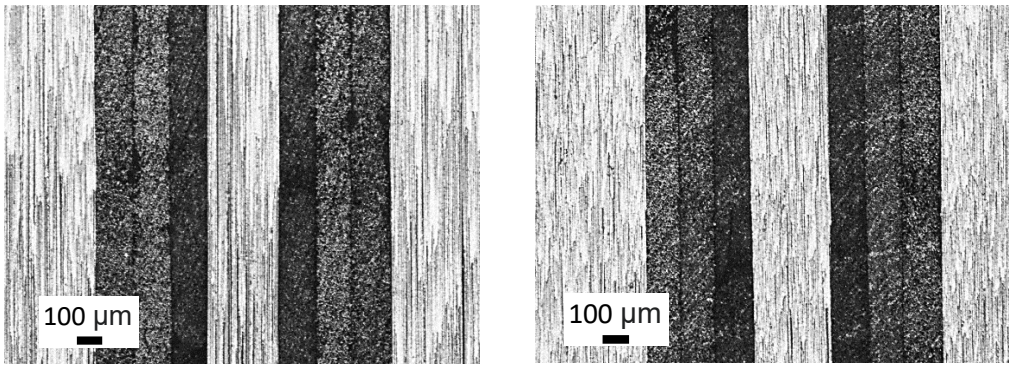

Figure 9. Micrographs of ground/polished Level 1 specimens.

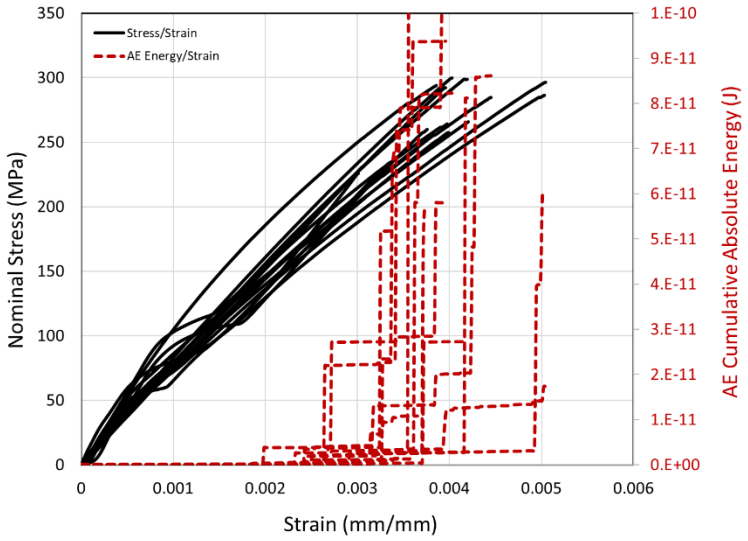

Figure 10. Nominal compression stress and AE responses for Level 2 characterization tests. (color on web only)

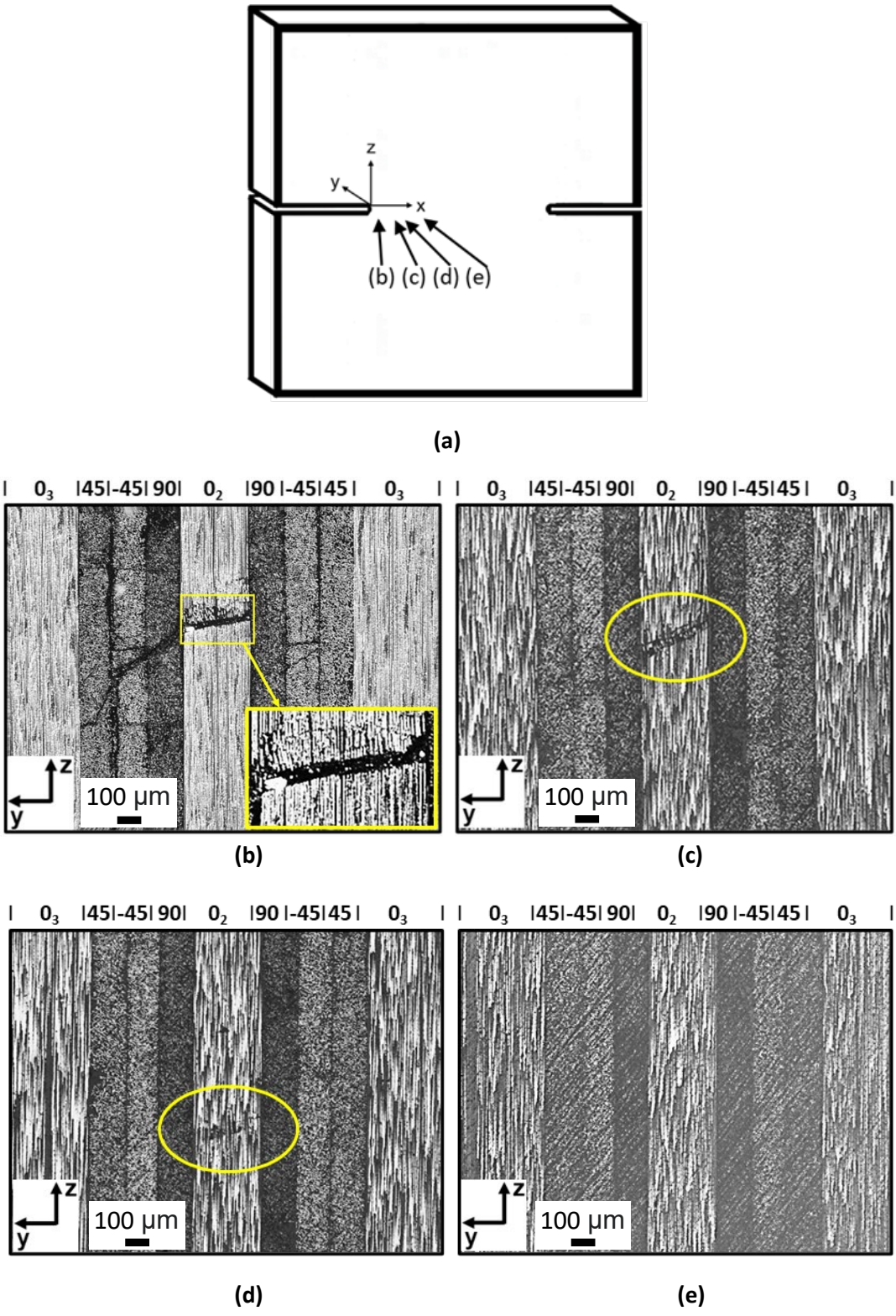

Figure 11. Micrographs of polished specimen at increasing distances (x) from the notch tip (a) specimen schematic, (b) 0.15 mm, (c) 2.2 mm, (d) 2.6 mm, and (e) 3.0 mm (color on web only)

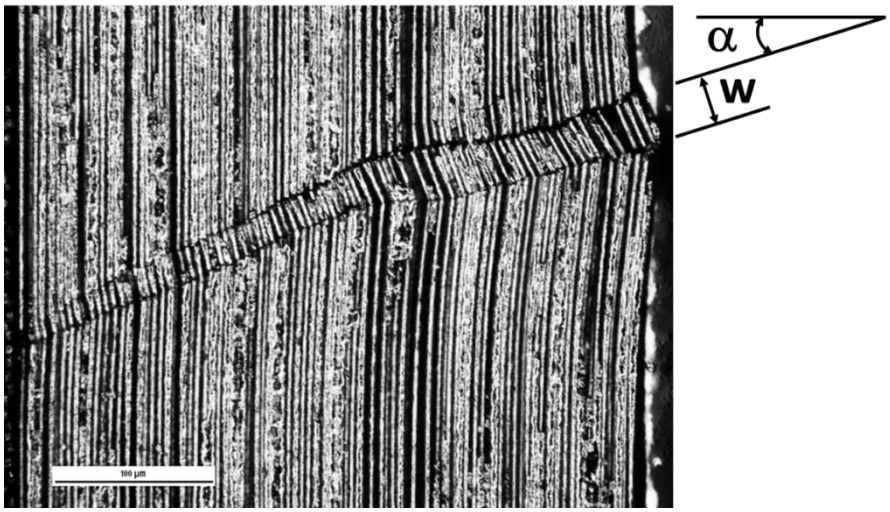

Figure 12. Micrograph of kink band with annotation of characterization parameters
(α = angle with respect to horizontal direction and w = kink band width)

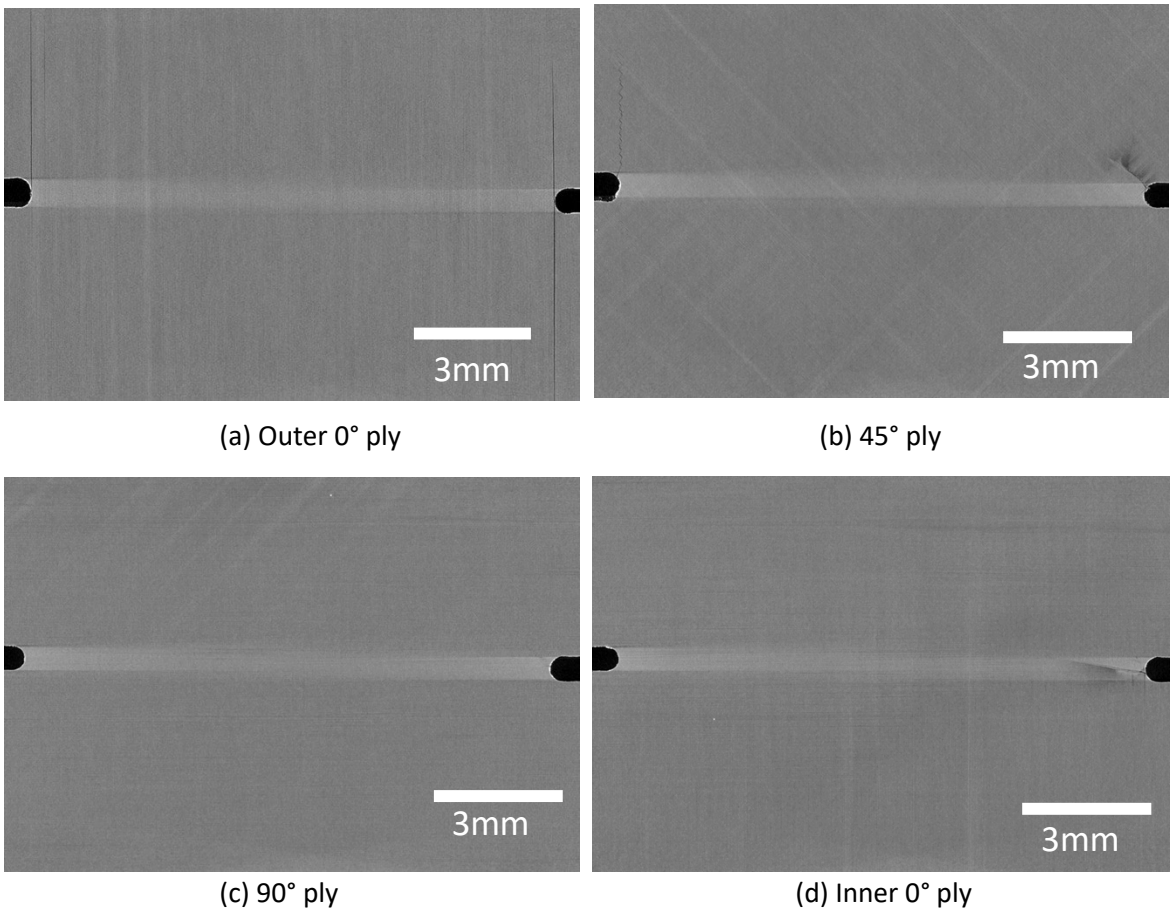

(a) Outer 0° ply (b) 45° ply

(c) 90° ply (d) Inner 0° ply

Figure 13. μCT images of four plies of damaged DENC specimen. Voxel size is 7.55 μm.

Figure 14. High magnification μCT tomograph of split/kink band in 45-degree ply (see Figure 13b). Voxel size is 2.55 μm.

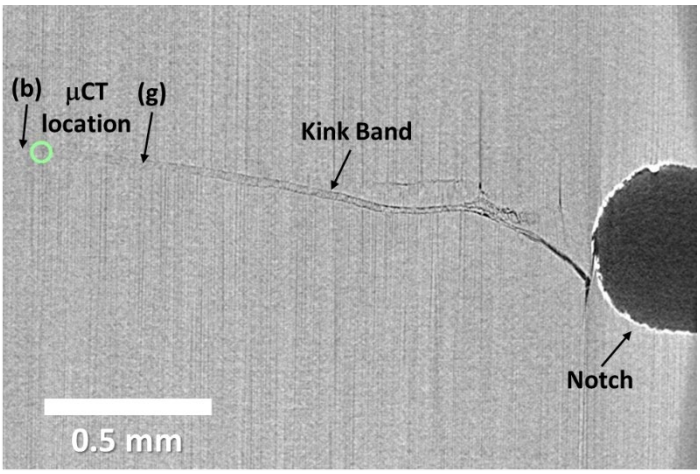

(a)

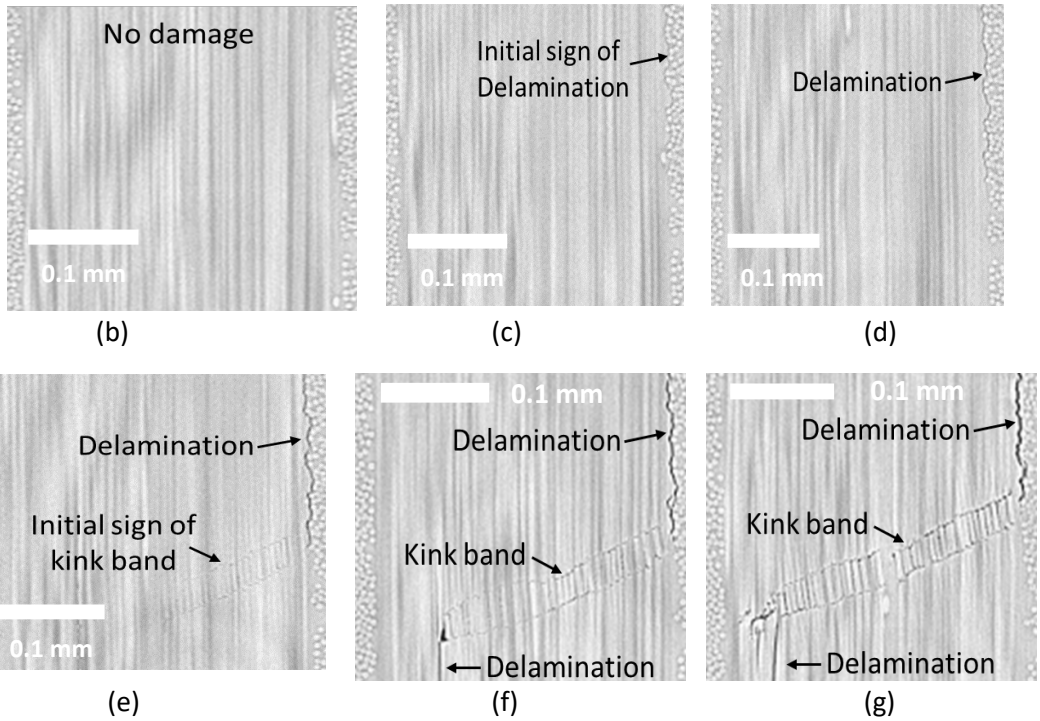

(b) (c) (d)

(e) (f) (g)

Figure 15. High magnification μCT tomographs of kink band in center zero-degree plies
(a) face view (see Figure 13d; voxel size of 2.55 μm), (b-g) through-thickness images progressing toward specimen notch (Voxel size of 0.395 μm)

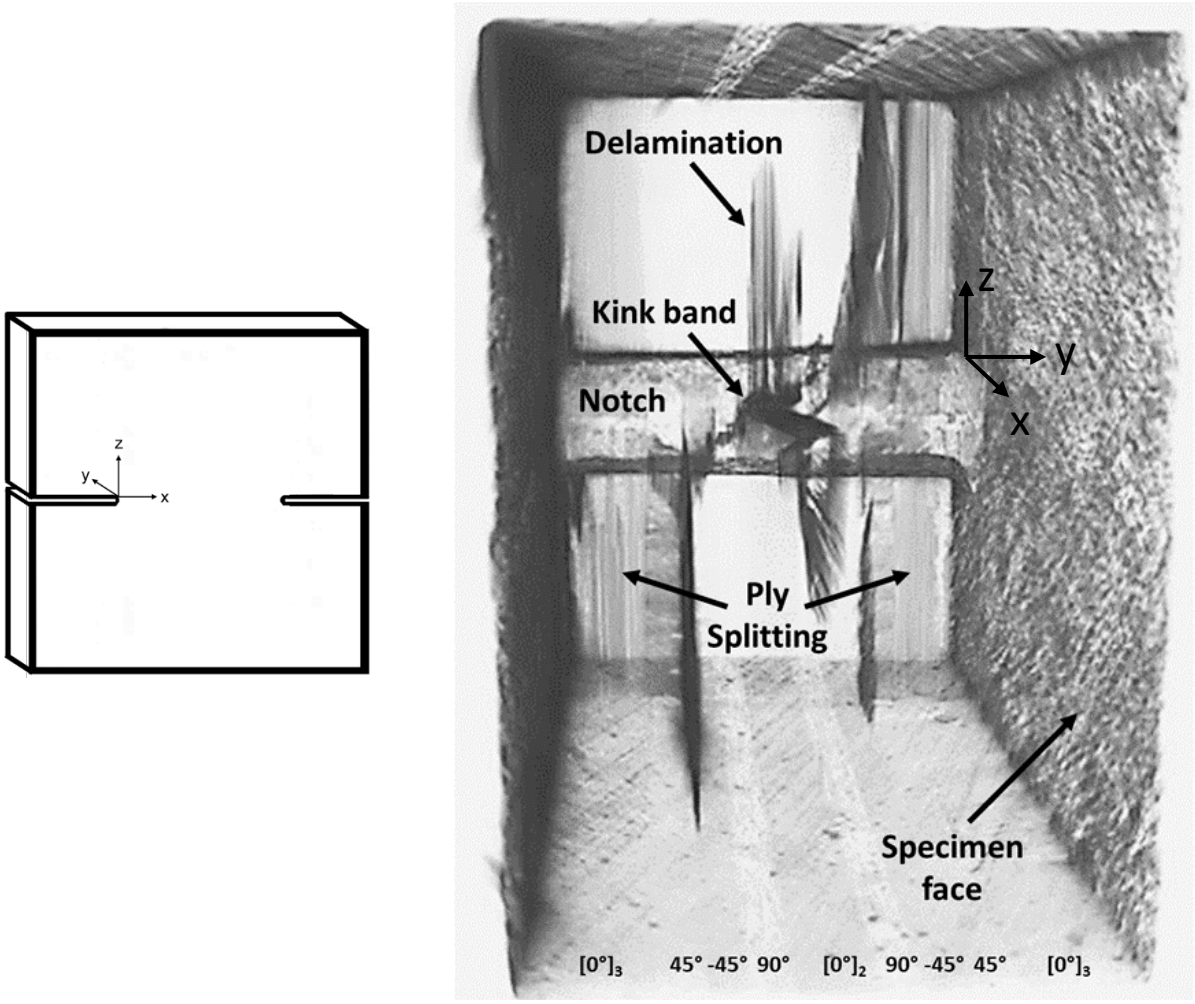

Figure 16. Three-dimensional μCT tomograph near notch of DENC specimen. The scan was performed using a dye-penetrant solution resulting in a voxel size of 7.55 μm.

Table 1. Mechanical properties of IM7/977-3

Property	Symbol	Mean	St Dev	ASTM
Compressive longitudinal modulus (GPa)	E_{1C}	137	0.608	D6641
Compressive transverse modulus (GPa)	E_{2C}	8.69	0.367	D3410
Compressive longitudinal strength (MPa)	X_C	1,569	44.2	D6641
Compressive transverse strength (MPa)	Y_C	248	11.3	D3410
Compressive longitudinal failure strain (%)	ε_{1C}	1.28	0.0586	D6641
Compressive transverse failure strain (%)	ε_{2C}	3.12	0.124	D3410
In-plane shear modulus (GPa)	G_{12}	5.01	0.249	D7078
Major Poisson's ratio	ν_{12}	0.320	0.0266	D3039

Table 2. Summary of Level 2 characterization test observations

Nominal Stress (MPa)	Max AE Event [aJ]	Experimental Observations
226	1.3E+05	Split from one notch tip
232	6.9E+04	Splits from both notch tips
234	2.2E+07	Horizontal crack from one notch tip
245	2.8E+06	Horizontal crack from one notch tip
257	8.9E+06	Splits from both notch tips + horizontal crack from one notch
260	2.4E+07	Large AE event
265	1.8E+08	Splits from both notch tips + horizontal crack connecting notches
266	1.3E+07	Large AE event
285	1.1E+07	Splits from both notch tips
286	2.0E+07	Large AE event
292	2.3E+07	Large AE event
294	4.0E+07	Splits from both notch tips
297	2.0E+06	Large AE event
299	2.2E+07	Splits from both notch tips
300	1.7E+07	Splits from both notch tips

Table 3. Kink band length, width, and angle of Level 2 characterization tests

Max nominal stress (MPa)	% Ultimate stress (%)	Length (x) range from notch tip (mm)	Kink band width (w) (mm)	Angle (α) with respect to horizontal (°)
234	74	1.0 – 1.6	0.023	21.0
285	90	1.6 – 2.4	0.029	23.5
294	92	2.6 – 3.0	0.029	21.5
297	93	0.7 – 2.8	0.024	27.0
299	94	0.8 – 1.6	0.023	23.0
300	94	2.1 – 2.9	0.020	23.0